https://doi.org/10.1093/plphys/kiad391 PLANT PHYSIOLOGY 2023: 193: 1365–1380

Plant Physiology®

Research Article

Photosystem II monomeric antenna CP26 plays a key role in nonphotochemical quenching in *Chlamydomonas*

Stefano Cazzaniga,[1] **Minjae Kim**,[2] **Matteo Pivato**,[1] **Federico Perozeni**,[1] **Samim Sardar**,[3] **Cosimo D'Andrea**,[3,4] **EonSeon Jin**[2,*] **and Matteo Ballottari**[1,*]

1 Dipartimento di Biotecnologie, Università di Verona, Verona 37134, Italy
2 Department of Life Science, Research Institute for Natural Sciences, Hanyang University, Seoul 04763, South Korea
3 Istituto Italiano di Tecnologia, Center for Nano Science and Technology, Milano 20134, Italy
4 Dipartimento di Fisica, Politecnico di Milano, Milano 20133, Italy

*Author for correspondence: matteo.ballottari@univr.it (M.B.), esjin@hanyang.ac.kr (E.J.)
The author responsible for distribution of materials integral to the findings presented in this article in accordance with the policy described in the Instructions for Authors (https://academic.oup.com/plphys/pages/General-Instructions) is Matteo Ballottari.

Abstract

Thermal dissipation of excess excitation energy, called nonphotochemical quenching (NPQ), is 1 of the main photoprotective mechanisms in oxygenic photosynthetic organisms. Here, we investigated the function of the monomeric photosystem II (PSII) antenna protein CP26 in photoprotection and light harvesting in *Chlamydomonas reinhardtii*, a model organism for green algae. We used CRISPR/Cas9 genome editing and complementation to generate *cp26* knockout mutants (named *k6#*) that did not negatively affect CP29 accumulation, which differed from previous *cp26* mutants, allowing us to compare mutants specifically deprived of CP26, CP29, or both. The absence of CP26 partially affected PSII activity, causing reduced growth at low or medium light but not at high irradiances. However, the main phenotype observed in *k6#* mutants was a more than 70% reduction of NPQ compared to the wild type (Wt). This phenotype was fully rescued by genetic complementation and complemented strains accumulating different levels of CP26, demonstrating that ~50% of CP26 content, compared to the Wt, was sufficient to restore the NPQ capacity. Our findings demonstrate a pivotal role for CP26 in NPQ induction, while CP29 is crucial for PSII activity. The genetic engineering of these 2 proteins could be a promising strategy to regulate the photosynthetic efficiency of microalgae under different light regimes.

Introduction

Photosynthetic complexes absorb photons and transfer electrons to redox reactions, leading to the synthesis of NADPH and ATP used to fix CO_2 into organic molecules (Hill and Scarisbrick 1940). Two photosystems are organized into 2 major moieties: reaction center (RC) and antenna subunits (Suga et al. 2015). Light-harvesting antenna proteins allow to increase the rate of light energy capture, efficiently transferring the excitation energy to the RC (Croce and Van Amerongen 2011). In limiting light conditions, this increased energy capture is crucial to maximize ATP and NADPH production, required for CO_2 fixation. However, increased light-harvesting capacity may become harmful upon exposure to high light (Long et al. 1994). An excessive light irradiance causes the saturation of the electron transport chain and overload of RCs, blocking or limiting the forward electron transport and preventing the photochemical use of the received energy. Limitation at the acceptor side can extend the lifetime of excited chlorophylls (Chls), increasing the probability of generating their triplet states. Triplets, in turn, can react with oxygen, causing the formation of reactive oxygen species (ROS) and leading to photodamage (Neidhardt et al. 1998). Photosystem II (PSII) RC components

Received April 14, 2023. Accepted June 06, 2023. Advance access publication July 5, 2023

are particularly sensitive to photodamage (Vass et al. 1992) with a specific repair cycle allowing to replace the damaged RC in the membrane (Aro et al. 1993). Photodamage can be related to excessive light but also to variable environmental conditions that could cause sudden changes in light irradiation (sun flecks), rapidly changing the number of photons received and transiently overloading the RCs (Graham et al. 2017). Moreover, possible overload of the photosynthetic apparatus can be a consequence of reduced regeneration of ADP and $NADP^+$ due to metabolic impairment or nutrient deficiency. Therefore, an efficient ability to regulate the energetic fluxes along the photosynthetic electron transport chain is a crucial requisite for the fitness of photosynthetic organisms. As a result, photosynthetic organisms need to constantly regulate the mechanisms of light capturing and utilization to maintain sufficient photochemical activity but avoiding photodamage (Erickson et al. 2015).

Evolution provides photosynthetic organisms with mechanisms to protect photosystems and preserve their functionality. Among these, the most responsive is the nonphotochemical quenching (NPQ) of Chls that rapidly dissipates the excess energy absorbed as heat, preventing triplet state formation (Horton 1996). NPQ response is triggered through a feedback mechanism by thylakoid lumen acidification, which is caused by saturation of the photosynthetic electron transport chain (Genty et al. 1989). Understanding the molecular mechanism of NPQ activation and deactivation processes has a great biotechnological relevance to improve the fitness and yield of photosynthetic organisms (Kromdijk et al. 2016; Głowacka et al. 2018). Microalgae are interesting for biotechnological applications, being photosynthetic microorganisms that can be cultivated in industrial environments such as biofactories for bioproducts of interest, like food additives, nutraceuticals, antioxidants, biostimulants, and even biofuels (Medipally et al. 2015; Bernaerts et al. 2019; Camacho et al. 2019; Koyande et al. 2019; Rani et al. 2021). In the model organism for green algae *Chlamydomonas reinhardtii*, the key proteins responsible for this mechanism activation are the pigment-binding proteins Light-Harvesting Complex Stress-Related 1 (LHCSR1) and LHCSR3 subunits, with the latter having a predominant role (Peers et al. 2009). Expression of LHCSR genes is strongly induced upon high light exposure. LHCSR proteins were reported to sense lumen acidification upon protonation of specific exposed residues, thus being able to switch from a light-harvesting state to a quenched 1 triggering NPQ (Peers et al. 2009; Liguori et al. 2013; Ballottari et al. 2016; Troiano et al. 2021).

While LHCSR is the trigger, it needs to interact with other antenna proteins of the photosystems to efficiently induce NPQ (Tokutsu and Minagawa 2013; Dinc et al. 2016). In *C. reinhardtii*, PSII light antennas are organized in 2 different moieties: trimeric major light-harvesting complexes (LHCII) and monomeric subunits (Shen et al. 2019). Trimeric LHCII are encoded by 9 genes, *lhcbm1* to *lhcbm9* (with M referring to "major" antenna complexes) (Minagawa and Takahashi 2004; Drop et al. 2014). Conversely, CP26 and CP29 are 2 monomeric LHC subunits that have a key role as a linker between the RC and the external LHCII (Drop et al. 2014; Semchonok et al. 2017; Cazzaniga et al. 2020). Indeed, the *C. reinhardtii* PSII homodimer RC is surrounded by 2 antenna layers (Tokutsu et al. 2012): the inner layer is composed of CP29, CP26, and S-LHCII (strongly bound), forming along with the core the C_2S_2 particle, whereas the outer layer is made of M-LHCII (moderately bound), forming along with C_2S_2 the $C_2S_2M_2$ supercomplex. An additional LHCII (N-LHCII) can be connected directly to the PSII core in the position that in vascular plants is occupied by the third monomeric antenna CP24 (absent in *C. reinhardtii*), forming the larger $C_2S_2M_2N_2$ (Drop et al. 2014).

The different LHC subunits have similar biochemical and biophysical properties (Natali and Croce 2015), but despite these structural similarities, different antennas have been suggested to have different roles in the light-harvesting mechanism and photoprotection. Indeed, the NPQ phenotype of specific *lhcbm* knockout or knockdown mutants led to the suggestion of specific roles in NPQ for LHCBM1 and LHCBM4-6-8. In the case of monomeric antenna LHC subunits, single mutants of CP26 or CP29 genes, called *k6* and *k9*, respectively, and a double CP26-and-CP29 mutant, called *k69*, were recently reported in *C. reinhardtii* showing a strong reduction of light-harvesting and NPQ mechanisms in the absence of both antenna proteins (Cazzaniga et al. 2020). However, in the *k6* mutant previously described, the absence of CP26 also caused the absence of CP29, resulting in a similar phenotype as the *k6* and *k69* mutants. Detailed information on the specific role of CP26 and CP29 in photoprotection and light harvesting are thus still missing. In this study, we further characterized the role of monomeric antennas in *C. reinhardtii* using CRISPR/Cas9 genome editing and complementation strategies, obtaining original *cp26* mutants (herein named *k6#*) where CP29 expression was similar to the wild type (Wt). The *k6#* mutants were characterized by partially reduced photosynthetic efficiency, reduced growth compared to its parental strain, and a strong impairment in NPQ induction. This finding, supported by genetic complementation, demonstrates an important difference between the function of CP26 in green algae and vascular plants: in the latter, the absence of CP26 had a minor effect, if any, on NPQ induction (de Bianchi et al. 2008).

Results

Analysis of CP26 and CP29 protein sequences

The protein sequences of CP26 and CP29 from *C. reinhardtii* are reported in Supplemental Fig. S1 aligned with the protein sequence of CP29 from spinach (*Spinacia oleracea*), for which a 3-dimensional protein structure was previously solved (Pan et al. 2011). CP26 and CP29 from *C. reinhardtii* share 40.52% sequence identity at the amino acid level, presenting large differences mainly at the N-terminus and in the loop before the predicted helix B. The putative Chl-binding residues identified in CP29 from spinach are conserved in both CP26 and

CP29 from *C. reinhardtii* except for the Chl614-binding residue (H), which is absent in CP29, while the Chl612-binding residue is histidine in CP29 (both from spinach and from *C. reinhardtii*) and asparagine in CP26, as previously reported in trimeric LHCII from plants (Liu et al. 2004). Interestingly, the tyrosine residue previously reported to be involved in neoxanthin binding is absent in CP26, suggesting a possible loss in this protein of the external N1 carotenoid–binding site, usually occupied by neoxanthin (Caffarri et al. 2007).

Expression of CP29 protein in the absence of CP26 and generation of CP26-deficient mutants in *Chlamydomonas*

The absence of CP29 in the previously reported *k6* mutant suggested a possible destabilization of CP29 binding to PSII in the absence of CP26 (Cazzaniga et al. 2020). To test this hypothesis, CP29 complementation was attempted in the double mutant *k69* background introducing the whole CP29 genomic sequence including the native promoter, 5′-UTR, 3′-UTR, and terminator (Supplemental Fig. S2). Complementation with the CP29 genomic sequence in the single mutant *k9* was performed as a control (Supplemental Fig. S3). Transformant lines successfully accumulated the CP29 subunit to a similar level compared to Wt in both *k9* and *k69* backgrounds, thus even in the absence of CP26 in the double mutant *k69*. While CP29 complementation of the single mutant *k9* fully restored the NPQ phenotype to the Wt level, this was not the case in the *k69* background, where despite CP29 accumulation, complemented strains were characterized by a strong reduction of NPQ similar to their background (*k69* mutant), suggesting a pivotal role for CP26 in NPQ. These findings prompted us to generate CP26 mutants to investigate the role of this antenna protein in *C. reinhardtii*. A reverse genetic approach was applied to knock out the CP26 gene (lhcb5, Cre16.g673650) in a Wt background through CRISPR/Cas9-mediated gene disruption (Baek et al. 2016; Kim et al. 2020a, 2020b) (Fig. 1). The sgRNA target located in exon 4 yielded successful results, leading to nonhomologous end joining and Cas9-mediated hygromycin-resistance (HygR; aphVII) gene cassette insertion in the target site (Fig. 1A). Insertion of the HygR gene cassette in the coding DNA sequence (CDS) of the target gene was confirmed by PCR and Sanger sequencing (Fig. 1; Supplemental Fig. S4 and Table S1), and the lines were named *k6#1* to *k6#11*. Ten mutants were validated by immunoblotting analysis with a specific antibody against CP26, confirming the absence

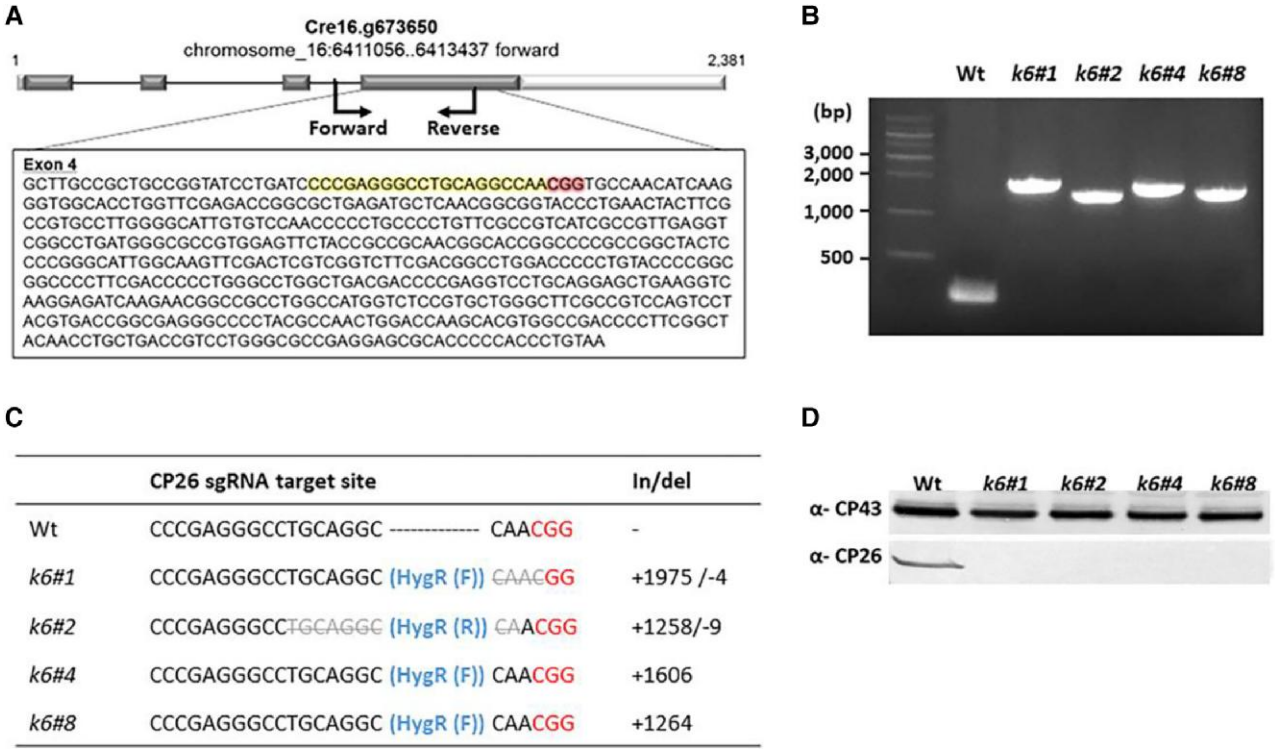

	CP26 sgRNA target site	In/del
Wt	CCCGAGGGCCTGCAGGC ---------- CAACGG	-
k6#1	CCCGAGGGCCTGCAGGC (HygR (F)) ~~CAACGG~~	+1975 /-4
k6#2	CCCGAGGGCC~~TGCAGGC~~ (HygR (R)) ~~CA~~ACGG	+1258/-9
k6#4	CCCGAGGGCCTGCAGGC (HygR (F)) CAACGG	+1606
k6#8	CCCGAGGGCCTGCAGGC (HygR (F)) CAACGG	+1264

Figure 1. CP26 knockout by CRISPR/Cas9 genome editing. **A)** Location of the Cas9 target site in the CP26 gene. Empty and solid boxes indicate UTR and exons, respectively. Nucleotides highlighted indicate the sgRNA sequence and its PAM sequence (CGG). Arrows indicate the primer sets for colony PCR. **B)** Colony PCR of the selected CP26 knockout mutants using the specific primers designed near the Cas9 target site of CP26. **C)** Sanger sequencing of the selected CP26 knockout mutants. In/del values represent inserted or deleted nucleotides in the sgRNA target site of CP26 in Wt. The hygromycin-resistance gene (HygR/aphVII) cassette inserted in the target site of the CP26 gene was identified with either forward (F) or reverse (R) orientation. The size of the HygR cassette is 1,624 bp. The CGG is reported and the deleted sequence in the sgRNA target site was crossed out. **D)** Immunoblotting analysis of the 4 selected CP26 knockout mutants with a specific antibody directed against CP26. Immunoblotting against CP43 was added as a loading control.

of the protein (Fig. 1D; Supplemental Fig. S3B). Southern blot analysis on the selected lines showed that *k6#4* and *k6#8* contained a single insertion of the HygR gene in the genome, while the others displayed multiple insertions (Supplemental Fig. S1C). These 2 mutants were considered for subsequent analysis.

Pigment content and pigment–protein complex stoichiometry in the mutant without CP26

Pigment content was analyzed in Wt and *k6#* cell cultures grown in photoautotrophy at 80 to 100 μmol m^{-2} s^{-1} for at least 3 generations (Table 1). The mutant, compared to its parental line, displayed a similar Chl content per cell but a slightly lower Chl *a*/*b* ratio. The Chl/carotenoid ratio and the carotenoid composition were comparable between the 2 genotypes, as confirmed by the HPLC analysis showing only minor and not significant differences in loroxanthin and antheraxanthin content. At this light intensity, zeaxanthin accumulation was not detected.

A partial rearrangement of the photosynthetic complexes in *k6#* lines could account for a lower Chl *a*/*b* ratio, being that Chl *b* is only bound by antenna subunits while Chl *a* is present in all pigment-binding complexes. To assess this hypothesis, we measured the relative amounts of PSI, PSII, LHCII, and CP29 using specific antibodies against the different photosynthetic subunits (Fig. 2). In particular, CP43 and PSAA were used as proxies for PSI and PSII content, respectively, while LHCII content was investigated using an antibody recognizing the different LHCBM subunits of *C. reinhardtii* (Girolomoni et al. 2017). Compared to Wt, the *k6#* mutant showed increased PSI/PSII and LHCII/PSII ratios. In particular, LHCII content per PSII was almost doubled, suggesting a possible compensation of the absence of monomeric antennas by an increase of the LHCII protein level (Fig. 2A). In the case of CP29, the CP29/PSII ratio was similar in *k6#* compared to Wt, as in the *k69* mutant complemented with CP29 (Supplemental Fig. S1). The organization of pigment-binding complexes was further analyzed by nondenaturing Deriphat-PAGE upon solubilization of thylakoid membranes with dodecyl-α-D-maltoside (α-DM) (Fig. 2C). Different pigment-binding bands were resolved: the *k6#* mutant showed a relative increase of the bands corresponding to antenna proteins and to PSI compared to the PSII core. It is important to note that the reduced Chl *a*/*b* ratio and the increased PSI/PSII and LHCII/PSII ratios observed in *k6#* are essentially in line with previous observations in the *C. reinhardtii* mutant *k9*, where CP29 was absent, while in the double mutant *k69*, the LHCII and PSI per PSII content were further increased (Cazzaniga et al. 2020). However, it is important to point out that while the CP29/PSII ratio was similar in *k6#* and Wt, in the *k9* mutant, an ∼50% increase in the CP26/PSII ratio compared to the Wt was observed (Supplemental Fig. S5), likely to partially compensate for the absence of CP29. Antenna proteins associate with core complex subunits that could be destabilized by the absence of monomeric antennas. Previous experiments using chemical cross-linking on thylakoids isolated from spinach have shown that CP26 interacts with the extrinsic PSII subunits of the oxygen-evolving complexes PSII subunit P (PSBP) and PSII subunit Q (PSBQ) (Ido et al. 2014). The PSBP content per PSII was thus analyzed by immunoblotting in the generated mutant strains: in the *k6#* mutant, an ∼30% reduction of the PSBP/CP43 ratio was observed compared to the Wt (Supplemental Fig. S6). An almost identical decrease of the PSBP/CP43 ratio was also detected in the *k9* mutant, while an ∼40% reduction was observed in the double mutant *k69* (Supplemental Fig. S6).

Light-harvesting efficiency

The consequences of CP26 absence on the activity of PSII were initially evaluated by measuring PSII maximum quantum efficiency (F_v/F_m) in dark-adapted cells (Butler 1973), revealing a significant decrease in the mutant (0.67 vs. 0.72 in *k6#* and Wt, respectively) (Table 1). Such difference is attributable to a higher basal fluorescence (F_0) in the mutant when exposed to weak measuring light, as reported by the fluorescence values normalized to the Chl amount (Supplemental Fig. S7): a higher F_0 value in *k6#* indicates that a fraction of the absorbed light energy is not efficiently directed toward photochemistry but reemitted as fluorescence. This alteration can be observed also by measuring fluorescence emission spectra at 77 K (Fig. 3A): *k6#* cells were characterized by an additional shoulder at ∼680 nm, usually assigned to "disconnected" LHC complexes, meaning LHC proteins are impaired in energy transfer to photosystems, thus reemitting fluorescence at shorter wavelengths (Garnier et al. 1986). The *k6#* mutant was thus characterized by an increased LHCII content, which however is partially not able to transfer energy to PSII: a similar phenotype could be observed in the absence of CP29 (*k9* mutant) or, to a greater extent, in the double mutant *k69*, without both CP26 and CP29 (Supplemental Fig. S8A), consistent with previous data

Table 1. Pigment analysis and F_v/F_m

	Chl (pg)/cell	Chl *a*/*b*	Chl/Car	F_v/F_m	Car/100 Chl					
					Neo	Lor	Viol	Ant	Lut	β-Car
Wt	1.40 ± 0.07	2.65 ± 0.04	3.16 ± 0.07	0.72 ± 0.01	3.43 ± 0.59	5.12 ± 0.36	3.30 ± 0.08	0.39 ± 0.04	13.85 ± 0.50	4.42 ± 0.71
k6#	1.47 ± 0.22	2.48 ± 0.04	3.16 ± 0.03	0.67 ± 0.02*	3.60 ± 0.96	3.99 ± 0.37	3.23 ± 0.27	0.15 ± 0.14	15.03 ± 0.90	4.21 ± 0.47

Data were collected from cells grown in photoautotrophy at 80 to 100 μmol photons m^{-2} s^{-1}. Single carotenoid values were normalized to 100 Chls. In the case of *k6#*, the results obtained were obtained from 2 independent mutant lines. Data are expressed as mean ± SD ($n = 4$). Values that are significantly different (Student's *t* test, $P < 0.05$) from the Wt are marked with an asterisk (*). Abbreviations: Chl, chlorophyll; Car, carotenoids; Neo, neoxanthin; Lor, loroxanthin; Viol, violaxanthin; Ant, antheraxanthin; Lut, lutein; β-Car, β-carotene.

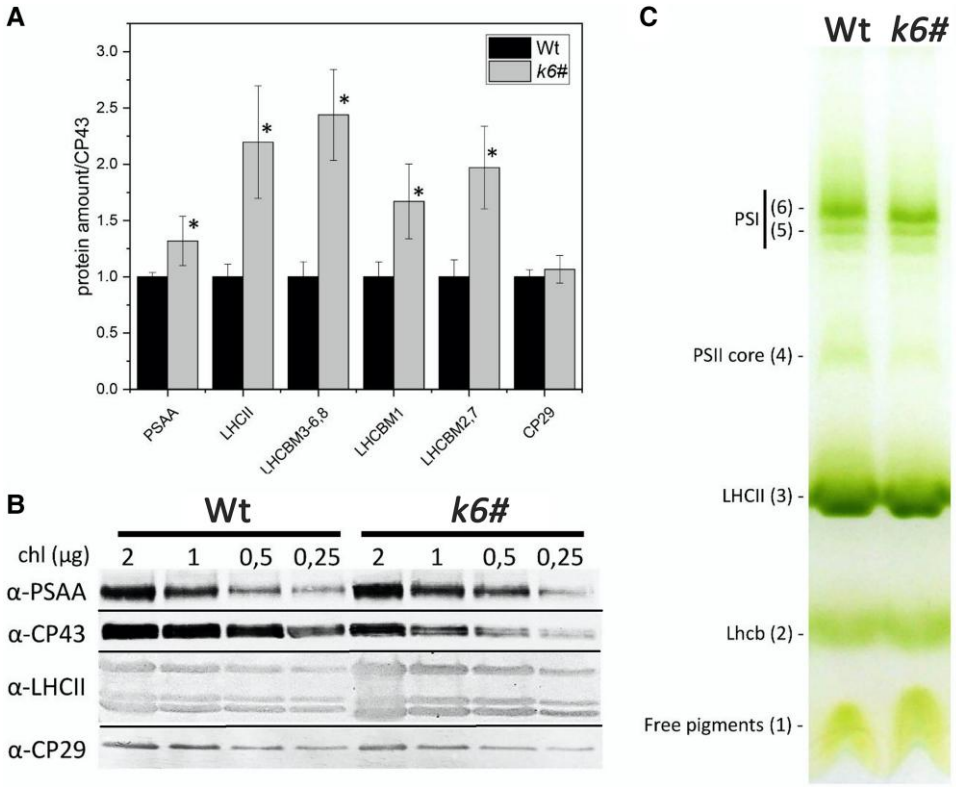

Figure 2. Organization of the photosynthetic complexes. **A)** Immunotitration of Wt and *k6#* thylakoid proteins using specific antibodies against the PSI core (PSAA), LHCII, and CP29. Data were corrected for the CP43 amount and normalized to the Wt ratio. LHCII is shown as the total amount (LHCII) or divided for 3 bands that are separated on the Tris-Tricine buffer system: the upper 1 corresponding to *lhcbm3* to *lhcbm6* and *lhcbm8* gene products, the 1 in the middle to *lhcbm1*, and the lower 1 to *lhcbm2* and *lhcbm7* (Girolomoni et al. 2017). Data are represented as mean ± SD ($n = 4$). *k6#* values that are significantly different (Student's *t* test, $P < 0.05$) from the Wt are marked with an asterisk (*). **B)** Image of western blotting used for the immunotitration. Specific antibodies were used on cellulose lanes loaded with 2, 1, 0.5, and 0.25 µg of Chls. **C)** Thylakoid pigment-binding complexes were separated by nondenaturing Deriphat-PAGE upon solubilization with 0.8% α-dodecyl-maltoside. Thylakoids corresponding to 30 µg of Chls were loaded in each lane. The composition of each band is indicated.

(Cazzaniga et al. 2020). The light-harvesting capacity of PSII, or functional PSII antenna size, was thus evaluated from the kinetics of Chl *a* fluorescence induction in whole cells in limiting light conditions upon treatment with the PSII inhibitor N-(3,4-dichlorophenyl)-N-dimethylurea (DCMU): in this condition, the rise time of Chl fluorescence is inversely proportional to the PSII light-harvesting feature (Malkin et al. 1981). *k6#* showed a functional antenna size similar to the Wt, even with a doubled LHCII/PSII ratio, further suggesting a reduced antenna-to-core energy transfer efficiency in this mutant (Fig. 3B). Energy transfer to the PSII RC was thus investigated on whole cells by measuring time-resolved fluorescence decay on Wt and *k6#* cells using 475-nm excitation (Fig. 3C). In the absence of CP26, the fluorescence decay traces were slower compared to the Wt. Similar results could be obtained in *k9* and *k69* (Supplemental Fig. S8B). As reported in Supplemental Table S2, fitting analysis with exponential functions allows to estimate the average lifetimes of fluorescence decay, which were increased in *k6*, *k9*, and *k69* compared to Wt, with the longest lifetime in the double mutant. These results confirm that in the absence of CP26, energy transfer from LHCII to the RC was partially impaired, with more evident consequences when both CP26 and CP29 were absent.

PSII photochemical activity was then investigated in *k6#* and its parental strain by measuring PSII operating efficiency (ΦPSII), PSII electron transport rate (ETR), and photochemical quenching (1 − qL) at different light intensities (Baker 2008). As reported in Fig. 4, these photosynthetic parameters were not significantly different between the Wt and *k6#* mutant. The only exception is represented by the ΦPSII at low light intensities, which was lower in *k6#* mutants. These results are different compared to *k9* and *k69*, where a strong reduction in the ETR and ΦPSII was observed, especially in the double mutant *k69* (Supplemental Fig. S8), consistent with previous findings (Cazzaniga et al. 2020). The influence of CP26 on light-dependent oxygen production was then investigated at different actinic light intensities (Fig. 4D). Despite having a similar maximum light-dependent oxygen production rate (Pmax), the *k6#* mutant was characterized by a reduced oxygen production at low and intermediate irradiances (Fig. 4D; Supplemental Table S3). The respiration in

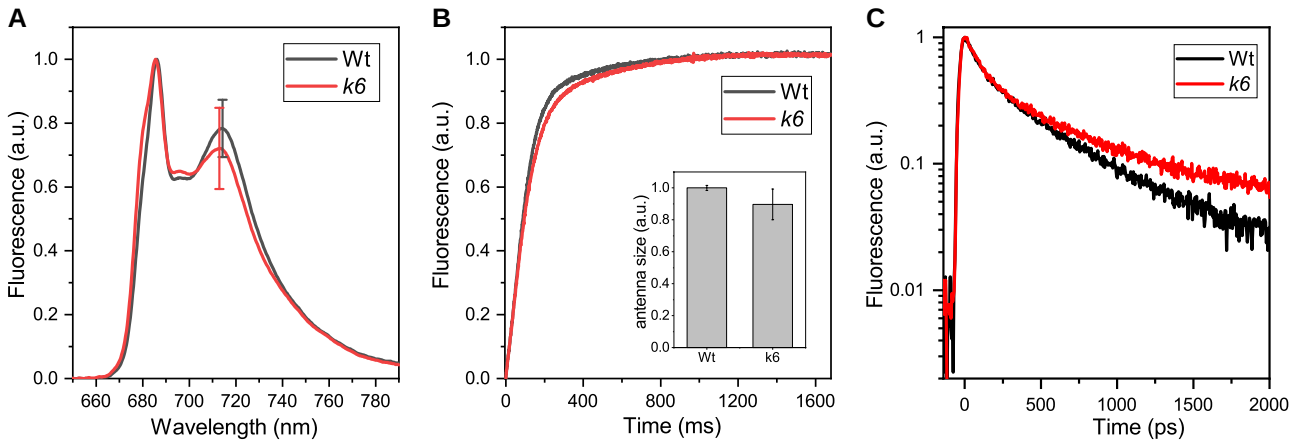

Figure 3. Light-harvesting properties of *k6#* mutants compared to Wt. **A)** Low-temperature fluorescence emission spectra of Wt (black) and *k6#* (red) cells excited at 475 nm. Emission spectra are normalized at the maximum emission on the PSII peak. Error bars are standard deviations ($n = 4$) indicated on the PSI peak. In the case of the *k6#* mutant, the results reported were obtained from 2 independent mutant lines. **B)** Variable Chl fluorescence was induced with a weak red light on dark-adapted cells ($2 \cdot 10^6$ cells/mL) in the presence of 50 μM of DCMU. The traces for Wt and *k6#* are the average of 12 curves from 3 different experiments. The reciprocal of time corresponding to two-thirds of the fluorescence rise ($1/\tau_{2/3}$) is a measure of the PSII functional antenna size and is shown in the inset normalized to the Wt. Error bars are standard deviations ($n = 12$). In the case of the *k6#* mutant, the results were reported from 2 independent mutant lines. **C)** Time-resolved fluorescence decay of Wt and *k6#* whole cells. In the case of the *k6#* mutant, the results reported in **A to C)** were obtained from 2 independent mutant lines.

the dark was not affected by CP26 absence (Supplemental Table S3). The partial destabilization of PSBP in *k6#* could be the reason for the reduced oxygen evolution when the light available is not saturating. However, a more evident decrease in oxygen production could be observed in the absence of CP29 in *k9* and even further in the double mutant *k69*, where the PSBP/CP43 content was similar to that in *k6#* (Supplemental Fig. S6). From these data, *k6#* showed a lower photochemical efficiency compared to Wt only at low–medium light, while a more severe reduction of PSII activity, even at high irradiances, could be observed in the absence of CP29 or both CP26 and CP29 (Supplemental Fig. S8).

Biomass productivity

To evaluate how these defects in *k6#* affect biomass yield, growth curves of both Wt and *k6#* strains were monitored in photoautotrophy at low (40 μmol m^{-2} s^{-1}), medium (80 to 100 μmol m^{-2} s^{-1}), and high lights (700 to 800 μmol m^{-2} s^{-1}) (Fig. 5). Under low or medium irradiances, the absence of CP26 caused a significant delay in the growth rate, reaching a cell density around half of the Wt in *k6#*. However, in the absence of CP29 (*k9* mutant) or both CP26 and CP29 (*k69* mutant), a much stronger reduction in biomass productivity could be observed (Supplemental Fig. S9). At higher light intensities, where light is not limiting, the growth curves of Wt, *k6*, *k9*, and *k69* strains were similar (Fig. 5C; Supplemental Fig. S9).

NPQ induction

Previous works demonstrated that the photoprotective induction of NPQ was essentially impaired in the absence of CP26 and CP29 but still active in the absence of CP29 only (Cazzaniga et al. 2020). The availability of a single *k6#* mutant depleted of CP26 allows us to investigate the specific function of this LHC in NPQ induction in *C. reinhardtii*. Because LHCSR proteins are required to induce NPQ (Peers et al. 2009), Wt and *k6#* strains were exposed to high light (1,200 μmol m^{-2} s^{-1}) for 2 d to induce LHCSR1 and LHCSR3 as previously reported (Allorent et al. 2013). Immunoblotting analysis revealed an increased content per PSII of both LHCSR1 and LHCSR3 in *k6#* compared to Wt (Supplemental Fig. S10). Despite the increased LHCSR content per PSII, NPQ induction in *k6#* was strongly reduced compared to the Wt with a residual NPQ ranging from ~6% at 150 μmol photons m^{-2} s^{-1} to ~30% at 2,400 μmol photons m^{-2} s^{-1} in the mutant (Fig. 6; Supplemental Fig. S11). In the same measuring conditions, NPQ was further reduced in the double mutant *k69* (Supplemental Fig. S12), with a residual NPQ compared to Wt ranging from 0% at 150 μmol photons m^{-2} s^{-1} to 10% at 2,400 μmol photons m^{-2} s^{-1}, consistent with previous findings (Cazzaniga et al. 2020). The absence of CP29 instead had a minor effect on NPQ with a residual NPQ compared to the Wt ranging from 50% at 150 μmol photons m^{-2} s^{-1} to 90% at 2,400 μmol photons m^{-2} s^{-1}.

NPQ is triggered by thylakoid lumen acidification. The NPQ phenotype observed in the *k6#* mutant could in principle be related to a reduced capacity in the mutant to generate a proton gradient across the thylakoid membrane upon illumination. To overcome this possible bias, light-independent NPQ activation was induced by direct lumen acidification by adding an acid solution to the cells as previously reported (Tian et al. 2019). Cells were first adapted to high light for 2 d to induce LHCSR, and then maximum

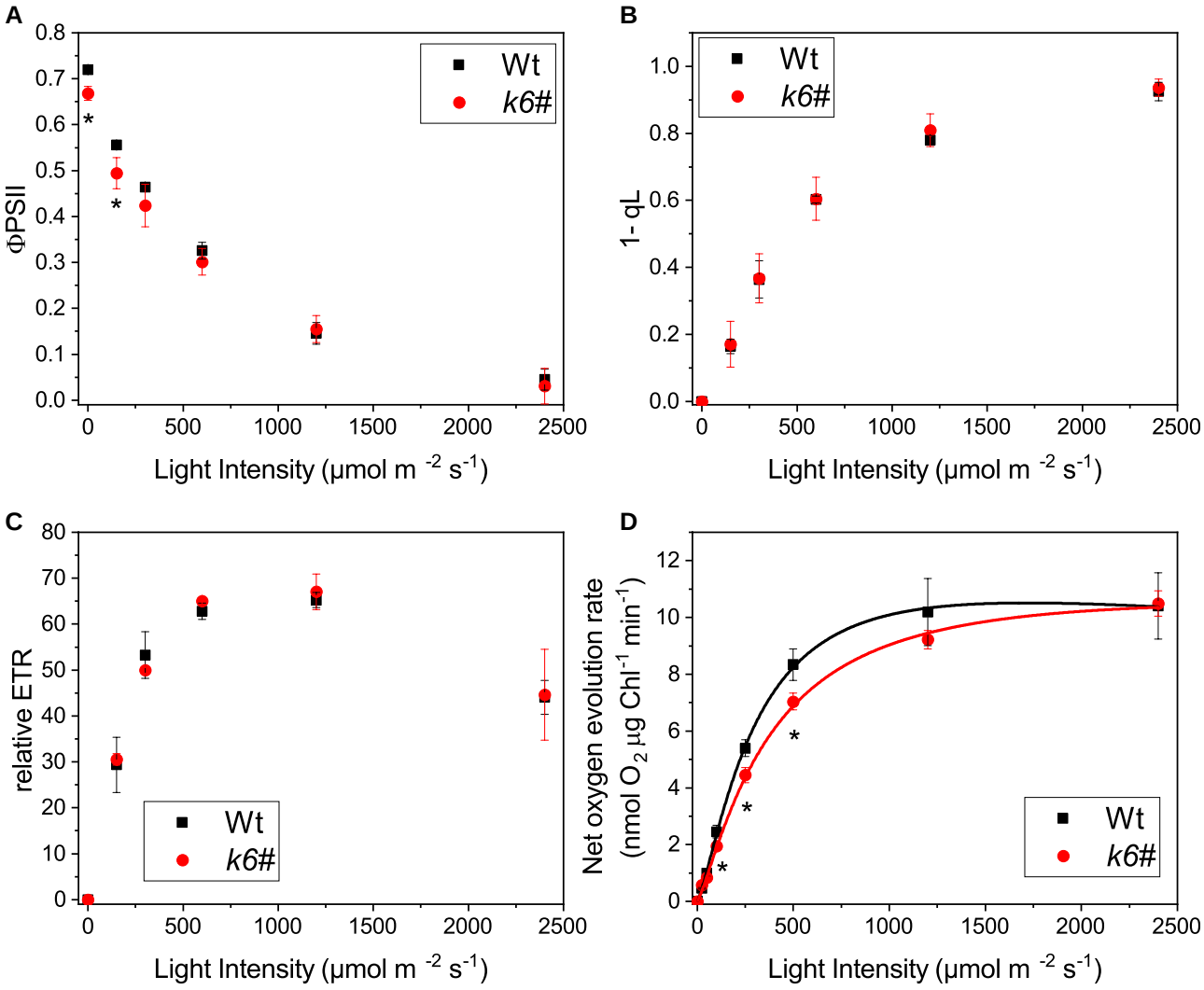

Figure 4. Photosynthetic electron flow in *k6#* mutants compared to Wt. Dependence of the **A)** ΦPSII, **B)** 1 − qL (reduced Q_A fraction), **C)** relative ETR, and **D)** photosynthetic O_2 evolution on actinic light intensity for Wt (squares) and *k6#* (circles). Net photosynthetic rate data were fitted with the Hill equation. In the case of the *k6#* mutant, the results reported were obtained from 2 independent mutant lines. Error bars are standard deviations ($n > 3$). *k6#* values that are significantly different (Student's *t* test, $P < 0.05$) from Wt are marked with an asterisk (*).

fluorescence emissions were measured by applying saturating pulses before (F_m) and after (F_m^a) decreasing the pH with an acid solution (Fig. 7). In the Wt, the acidification induced a strong decrease of F_m^a compared to F_m with a calculated NPQ of 1.76, whereas in *k6#*, the same procedure induced only a limited decrease of the F_m^a and a NPQ of 0.52. These differences between Wt and *k6#* are comparable to the ones obtained inducing NPQ by light exposure, further suggesting that the impaired quenching in *k6#* is mainly caused by a hampered NPQ mechanism rather than an impairment in the thylakoid lumen acidification. To validate the procedure, we tested direct acidification on a null NPQ mutant (*npq4 lhcsr1*, lacking both LHCSR1 and LHCSR3) and its parental strain (4a+), observing an absence of pH-dependent quenching in the absence of LHCSR subunits (Supplemental Fig. S13). The same approach tested on *k9* and *k69* cells showed that the mutant without CP29 had a level of NPQ similar to Wt, while the double mutant *k69* showed a strongly reduced level of quenching (Supplemental Fig. S14).

Genetic complementation of the *k6#* mutant

A genetic complementation approach was performed to associate the observed phenotypes with the absence of CP26. First, we tried to use the whole CP26 genomic sequence including the native promoter, 5′-UTR, 3′-UTR, and terminator (Supplemental Fig. S15). However, we were unable to synthesize or amplify the 1,000-bp upstream of the CDS due to its complexity and the presence of an unsequenced region in the genome. To overcome this issue, we decided to exploit the 1,000-bp upstream region of the other monomeric antenna CP29 (Cre17.g720250) as a putative promoter, which did not pose the same challenge as the CP26 region. This

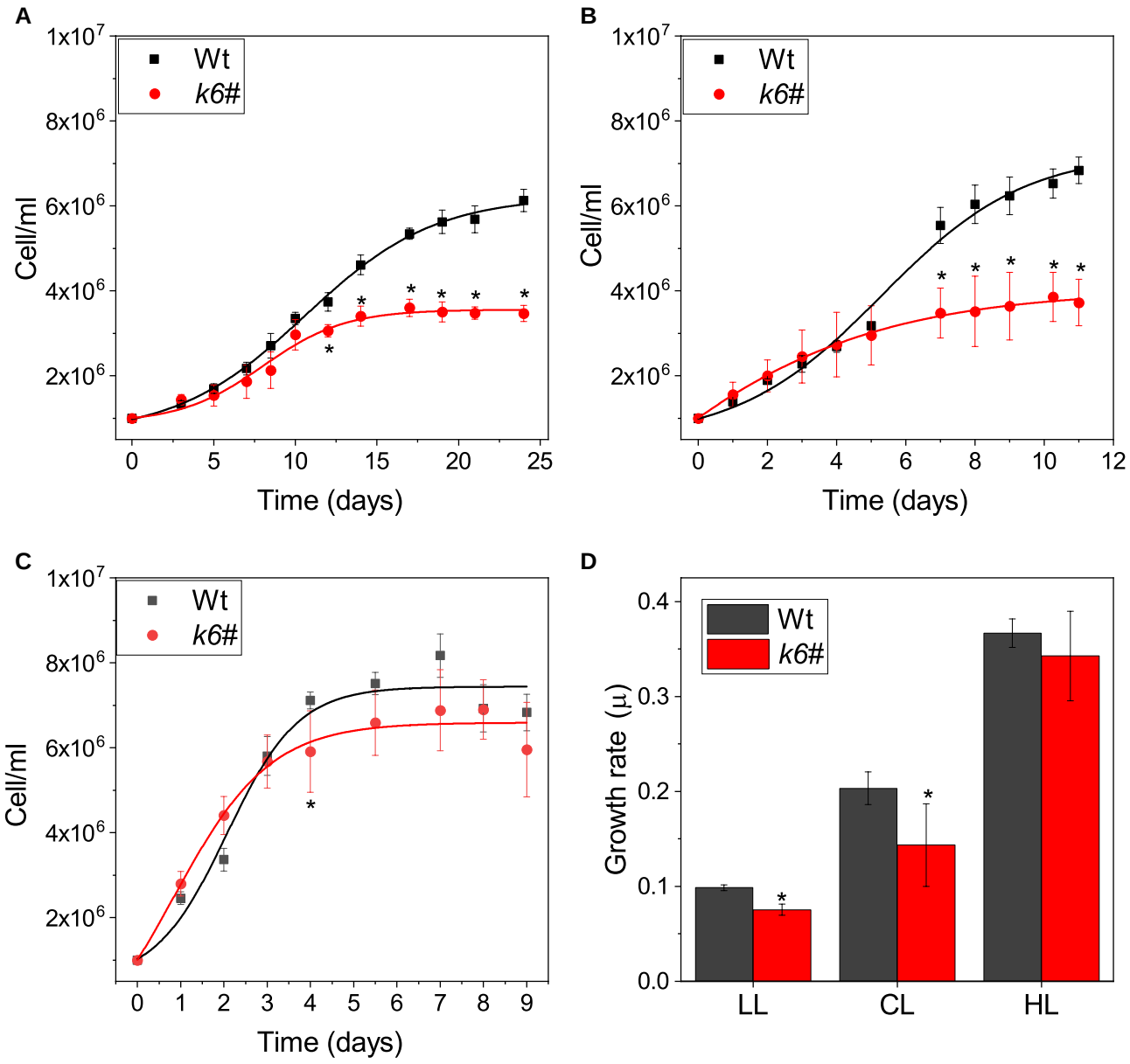

Figure 5. Growth curves under autotrophic conditions. Wt (squares) and *k6#* (circles) where grown at **A)** low (30 to 40 μmol m^{-2} s^{-1}, LL), **B)** control (100 to 120 μmol m^{-2} s^{-1}, CL), or **C**) high light (700 to 800 μmol m^{-2} s^{-1}, HL), and the cell content was measured. Growth curves were fitted with the Hill equation. **D)** Specific growth rate (μ) calculated for all the different light conditions. Error bars are standard deviations ($n > 3$). *k6#* values that are significantly different (Student's *t* test, $P < 0.05$) from Wt are marked with an asterisk (*). In the case of the *k6#* mutant, the results reported were obtained from 2 independent mutant lines.

chimeric construct (CP29, 1,000-bp upstream–CP26 gene from 5′-UTR to 3′-UTR–CP26, 300-bp downstream) was then introduced in the *k6#8* mutant line, resulting in the successful accumulation of CP26 protein. The CP26-expressing lines in the *k6#* background were named *k6#c* (*ko cp26* complemented): different levels of CP26 expression were observed in *k6#c* lines, ranging from ∼10% to 200% of the Wt CP26/PSII ratio (Supplemental Fig. S16). Five lines with a CP26/PSII ratio identical to the Wt were selected and renamed *k6#c1* to *k6#c5*. These lines were characterized by their pigment content, light-harvesting efficiency, and biomass productivity. In *k6#c*, the amount of Chl per cell and the Chl *a*/*b* and Chl/carotenoid ratios were identical to those in the Wt (Supplemental Table S4), recovering the small pigment changes associated with CP26 absence in the *k6#* mutant (Table 1). In the case of PSII maximum quantum efficiency, the reduced F_v/F_m values observed in *k6#* mutants were not observed in complemented *k6#c* lines, which showed an F_v/F_m almost identical to the Wt (Supplemental Table S4). Consistently, the ΦPSII at the lower actinic light intensities, which was lower in *k6#*, reverted to a value identical to the Wt in the complemented *k6#c* lines (Supplemental

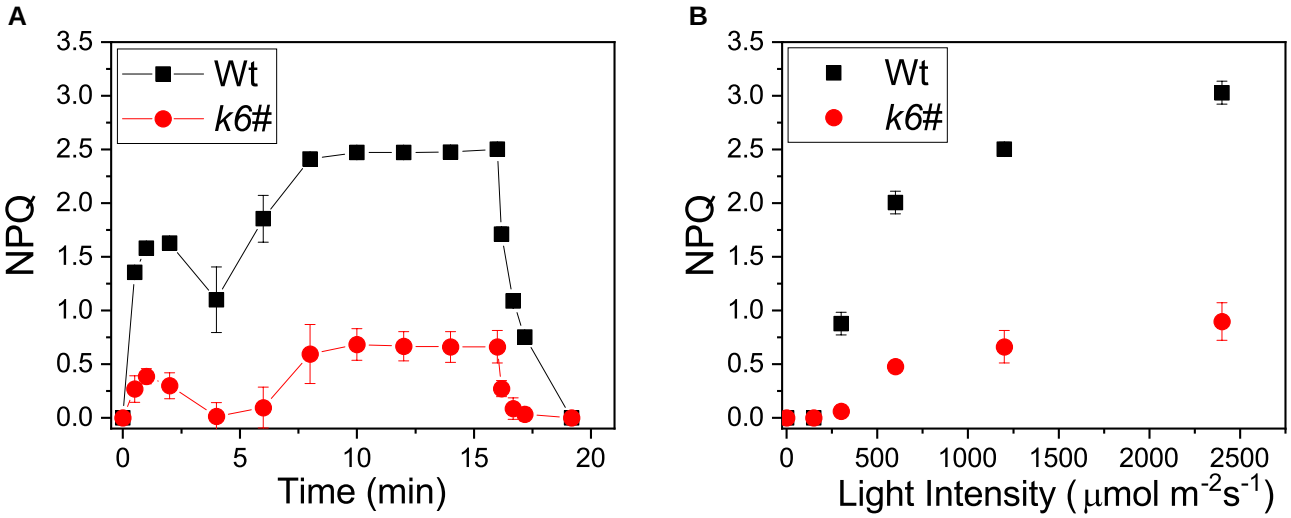

Figure 6. NPQ in *k6#* mutants compared to Wt. **A)** Measurement of NPQ kinetic on Wt (squares) and *k6#* (circles) cells using actinic lights of 1,200 μmol photons m^{-2} s^{-1}. **B)** NPQ value after 15 min of illumination at different actinic light intensities. Error bars are standard deviations ($n > 4$). In the case of the *k6#* mutant, the results reported were obtained from 2 independent mutant lines.

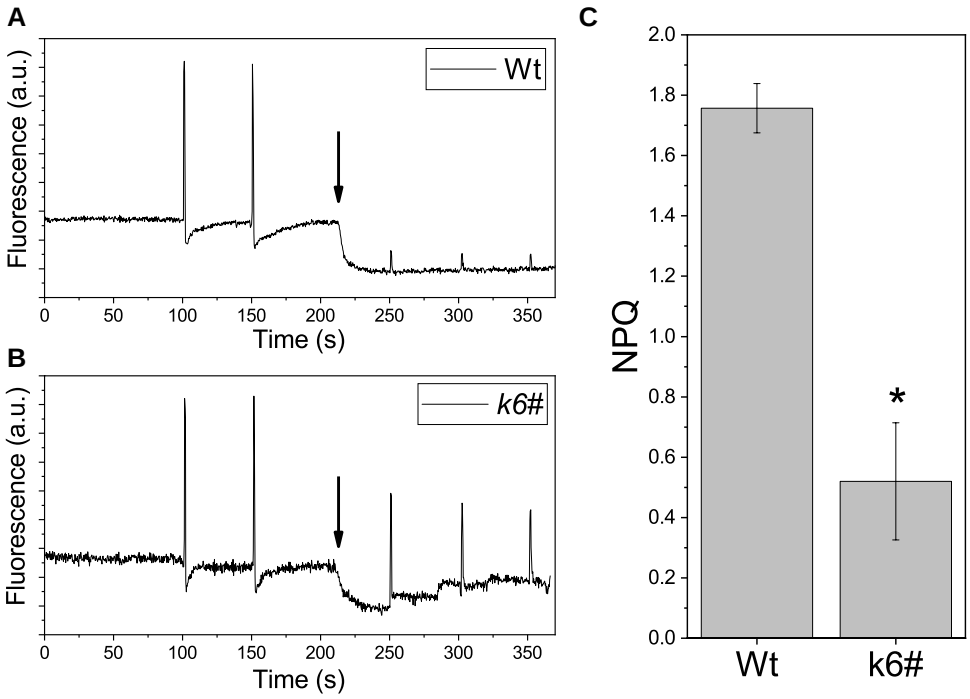

Figure 7. Acid-induced quenching in *k6#* mutants compared to Wt. **A, B)** PAM Chl fluorometer traces of Wt **A)** and *k6#* **B)** before and after acidification with acetic acid. The arrow indicates when the acid was added. Fluorescence was recorded in the dark with 2 saturating pulses before and 2 after the acidification. **C)** NPQ calculated for each trace as $(F_m - F^a_m)/F^a_m$, where F_m and F^a_m are the fluorescence before and after acidification. Error bars are standard deviations ($n > 3$). *k6#* values that are significantly different (Student's *t* test, $P < 0.05$) from Wt are marked with an asterisk (*).

Fig. S17). The light-dependent oxygen evolution, investigated at different actinic light intensities, was also similar between Wt and *k6#c*, while *k6#* showed a reduced oxygen production at light intensities between 150 and 1,200 μmol m^{-2} s^{-1}.

The complemented lines were tested also for biomass productivity growing cells at the 3 different light intensities described before (low, medium, and high lights) (Supplemental Fig. S18). At all 3 light intensities tested, the complemented *k6#c* lines showed a growth rate identical to the Wt, recovering the reduced growth phenotype at low and medium light intensities observed in the *k6#* mutant.

The NPQ phenotype of *k6#c* complemented lines was then investigated and compared to the *k6#* mutant and Wt. *k6#c* lines were adapted for 2 d in high light, and NPQ was

measured upon exposure to 1,200 μmol photons m^{-2} s^{-1} actinic light. As reported in Fig. 8A, in the case of *k6#c* complemented lines, the NPQ induction kinetics were similar between Wt and the selected *k6#c* lines, highlighting that the NPQ phenotype in *k6#* was specifically due to the absence of CP26. NPQ values obtained for the different complemented lines expressing different levels of CP26 were then plotted as a function of the CP26/PSII ratio considering also other *k6#c* lines with different levels of CP26 accumulation (Fig. 8B). When the CP26 content per PSII was at least 50% of that of the Wt, the NPQ induction capability was saturated and similar to the Wt. These data confirm the crucial role of CP26 in the mechanism underlying NPQ in *C. reinhardtii*, indicating that half of the CP26/PSII content observed in Wt is sufficient to ensure the complete activation of this photoprotective mechanism.

Discussion

In a previous study, we analyzed the effect of the absence of CP29 or both CP26 and CP29 in *C. reinhardtii* (Cazzaniga et al. 2020). The simultaneous absence of CP26 and CP29 affected both photosynthetic efficiency and photoprotection with an almost complete impairment of NPQ induction (Cazzaniga et al. 2020). However, a comprehensive study of the specific role of CP26 protein in light-harvesting and NPQ mechanisms still lacked so far. The CRISPR/Cas9 approach attempted in our previous work to obtain a single *cp26* mutant indeed resulted in the absence of both CP26 and CP29 (Cazzaniga et al. 2020), leading to the suggestion of a possible destabilization of CP29 accumulation in the absence of CP26. However, when we complemented the double mutant *k69* with CP29 only, it was possible to obtain complemented strains expressing CP29 even in the absence of CP26, confuting our previous hypothesis (Supplemental Fig. S1). On the basis of our findings, we can thus suggest that the absence of CP29 in the lines generated by CRISPR/Cas9 targeted to the *CP26* gene in our previous work (Cazzaniga et al. 2020) was likely related to some off-target mutations at the level of the *CP29* gene or to some other genes, which control the expression of CP29 at the translational or posttranslational level. We cannot exclude that some off-target mutations might be present also in the *k69* mutant, where the CP26 mutation was generated as in the case of the previous *k6* mutant, but these mutations are extremely difficult to be detected and properly evaluated. This result suggested to further investigate the role of CP26 in *C. reinhardtii* by selecting different target regions for Cas9 activity to obtain mutants depleted of this minor LHC protein. Here, the availability of a single *k6#* mutant and its complemented lines allow us to investigate the effects of the lack of this monomeric antenna on photosynthesis and cell physiology. In the complemented lines, the phenotypes observed in the *k6#* mutant on pigment accumulation, PSII activity, oxygen evolution, biomass productivity, and NPQ induction were recovered to the Wt level (Supplemental Figs. S16 and S17), confirming that these phenotypes were specifically due to the absence of CP26 in *k6#* lines.

In the absence of CP26, F_v/F_m was lower due to an increase of F_0 fluorescence, and the low-temperature fluorescence showed a shoulder around 680 nm that represents defectively connected LHCII (Fig. 3). Similar results were obtained in the absence of CP29 in the *k9* mutant and were even more evident in the double mutant *k69* (Supplemental Figure S8A). These data imply a reorganization of the PSII supercomplex in the absence of monomeric antenna subunits, with a reduced efficiency of energy transfer from a portion of the antenna system to the core. Accordingly,

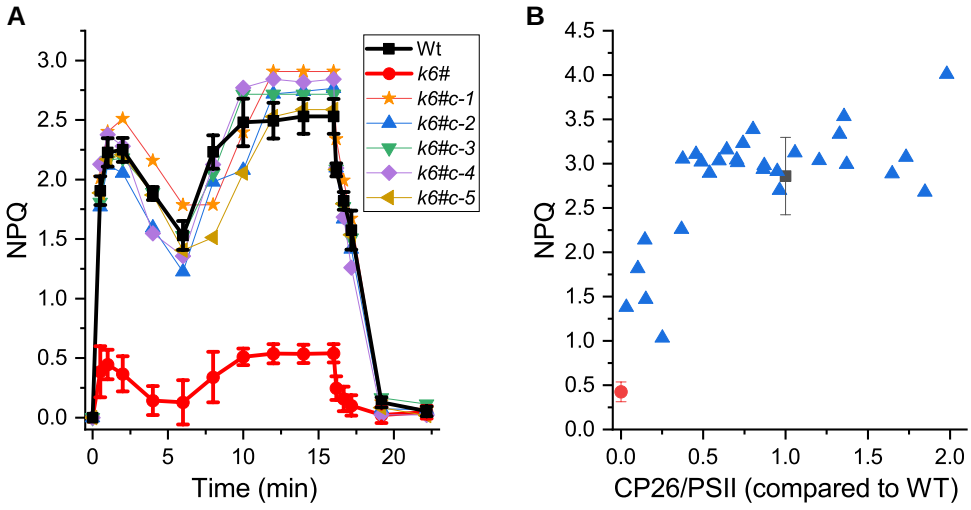

Figure 8. NPQ in the *k6#* complemented lines. **A)** NPQ using an actinic light of 1,200 μmol m^{-2} s^{-1} in 5 *k6#* lines complemented with CP26. The selected lines (named *k6#c1* to *k6#c5*) accumulate CP26 to the same level as the Wt. Wt (squares) and *k6#* (circles) NPQ traces were added as references. **B)** Association between the amount of CP26 and the NPQ reached after 15 min of illumination with actinic light at 1,200 μmol m^{-2} s^{-1}. Different *k6#c* lines are indicated as blue triangles, Wt as a black square, and *k6#* as a red circle. Error bars are standard deviations ($n = 3$).

time-resolved fluorescence analysis on whole cells demonstrated a reduced energy transfer from PSII antenna complexes to the RC in the absence of CP26, CP29, or both (Fig. 3C; Supplemental Fig. S8B). Moreover, in *k6#*, the LHCII content was strongly increased compared to Wt (Fig. 2), similar to a previous result on the single mutant *k9*, even if a further increased LHCII content was observed in the double mutant *k69* strains (Cazzaniga et al. 2020). This compensatory increase in LHCII was not entirely successful for all mutant strains, as can be seen by the appearance of fluorescence signatures at 77 K related to "unconnected" LHCII in the absence of CP26, CP29, or both. Moreover, in *k6#*, the functional antenna size was similar to the Wt even if the amount of LHCII was almost doubled (Fig. 3). It is important to note that "unconnected" LHCII has a higher fluorescence yield compared to LHCII connected to PSII, making the 77-K spectra not suitable to investigate the PSI/PSII ratio in *k6#* mutants: indeed, despite a similar ratio between the PSI and PSII peaks in the 77-K spectra between Wt and *k6#* mutants (Fig. 3), the immunoblotting analysis demonstrated a 30% increase in PSI/PSII in the absence of CP26 (Fig. 2). The reduced energy transfer efficiency in the absence of CP26 influenced the photosynthetic activity of PSII, causing reduced light-dependent oxygen evolution, especially at low–medium irradiances (Fig. 4; Supplemental Table S3). The absence of CP29 and/or CP29 caused the partial destabilization of the oxygen-evolving complex subunit PSBP (Supplemental Fig. S6) and possibly of other subunits such as PSBQ or PSBR. The destabilization of extrinsic subunits involved in oxygen evolution might partially explain the reduced light-dependent oxygen production observed in the *k6#* mutant, restored in the complemented *k6#c* lines. However, the similar Pmax of Wt and *k6#* mutants suggests that proper PSII photochemical activity can be restored even in the absence of CP26, providing increased photons to counterbalance the reduced light-harvesting efficiency observed in the mutant. These results differ from that of the mutant strains without CP29 (*k9* and *k69*), where despite a similar destabilization of PSBP compared to *#k6* mutants, the oxygen evolution rates were always lower than Wt and *#k6*, resulting in reduced Pmax.

The altered photosynthetic activity in the absence of CP26 also affected biomass accumulation when grown in limiting light conditions, where the *k6#* exhibited a lower cellular density and the growth rate was reduced compared to Wt. However, a more severe reduction in the growth rate could be observed in the case of *k9* and *k69* (Supplemental Fig. S9), consistent with the lower photosynthetic activity measured in the absence of CP29 or both CP26 and CP29 compared to the case where only CP26 was missing. These phenotypes on biomass productivity could be at least partially related to the destabilization of PSBP in *k6#*, *k9*, and *k69* mutants limiting PSII activity. However, when mutant strains were grown at higher light intensities (700 to 800 μmol m^{-2} s^{-1}), similar growth curves were observed for Wt and mutant strains, suggesting that in these conditions, light harvesting and PSII activity were not limiting the growth. All these data point out that both monomeric antenna proteins are important for efficient light harvesting in *C. reinhardtii* but CP29 has a prominent role. These functional differences associate with the position of the 2 antennas in the PSII supercomplex: CP29 is located in the inner layer of the antenna and interacts with trimers S-LHCII and M-LHCII and marginally with additional N-LHCII, while CP26 is in a more external position and interacts only with S-LHCII that is still connected to the RC from the other side through CP29 (Shen et al. 2019). Due to this organization, the absence of CP29 had a stronger impact on PSII antenna complexes and on the efficiency of energy trasfer to the core complex. Our data indicate that CP26 not only interacts with PSBP, as already suggested (Ido et al. 2014), but that monomeric antennas are also important for its accumulation and/or stability. Detailed study of other PSII subunits and direct structural analysis, by crystallography or cryo-EM, will be further required to reveal the detailed relationships between CP26, CP29, PSBP, and other core subunits.

Photosynthetic organisms evolved specific strategies to maximize light harvesting in low light conditions and avoid excess energy absorption in high light. In the case of the model organism for green algae *C. reinhardtii*, NPQ induction requires the presence of LHCSR proteins, which, upon thylakoid lumen acidification, are activated through their pH-sensing residues (Liguori et al. 2013; Ballottari et al. 2016). LHCSR proteins need to interact with other antenna proteins to efficiently redirect and quench the excess light energy absorbed (Liguori et al. 2013; Ballottari et al. 2016). Alternatively, it cannot be excluded that LHCSR can trigger a conformational change in other antenna subunits, leading to the formation of additional energy dissipation sites (Tokutsu and Minagawa 2013). Previous works demonstrated by electron microscopy the interaction of LHCSR3 dimers with CP26 and LHCII subunits, but the specific functions of the different antenna proteins in the NPQ process have not been fully elucidated yet. In the case of LHCII, the absence of LHCBM1 (Elrad et al. 2002) or downregulation of LHCBM4-6-8 subunits (Girolomoni et al. 2017) caused a reduction of NPQ induction, suggesting these subunits as potential partners for LHCSR3. Our previous findings demonstrated that in the absence of monomeric CP26 and CP29 subunits, NPQ induction was essentially impaired in *C. reinhardtii* (Cazzaniga et al. 2020). Here, we can narrow down our knowledge, demonstrating a specific function for CP26 in NPQ (Fig. 6; Supplemental Fig. S11). The absence of CP29 in *k9* also caused a decrease in NPQ compared to Wt but to a lesser extent compared to that in *k6#*, while a more dramatic NPQ phenotype was observed in the absence of both CP26 and CP29 subunits in the *k69* mutant (Supplemental Fig. S11). The impaired NPQ mechanism in *k6#* could be due to a decreased LHCSR/LHCII ratio, which was reduced in *k6#* compared to that in Wt. The relatively reduced LHCSR/LHCII stoichiometry in *k6#* could indicate a lower possibility to quench the increased amount of trimers

in the absence of CP26, resulting in a lower level of NPQ. However, in the *k9*, the LHCSR/LHCII ratio was similar to that in *k6#* (Cazzaniga et al. 2020), but the NPQ induction was less affected. Thus, reduced NPQ in the absence of CP26 may not be due to the alteration of the LHCSR/LHCII ratio. Different lumen acidification could also be excluded as a possible explanation for reduced NPQ observed in *k6*, according to the similar NPQ impairment observed upon induction of NPQ in the dark by artificial lumen acidification. The specific role of CP26 in NPQ was confirmed by the genetic complementation of *k6#* mutants (Fig. 8). Interestingly, the accumulation of CP26 per PSII to a 50% level compared to the Wt case was sufficient to fully restore NPQ. PSII supercomplexes are included in the tightly stacked grana of the thylakoid membranes, and a single PSII can pair up with near complexes or connect with complexes across the stromal gap (Albanese et al. 2017). It is possible to speculate that these close interactions may allow CP26 to interact with different complexes, reducing the amount needed of this subunit to transfer excitation energy from PSII to the quenchers, as LHCSR proteins. These data confirm the fundamental importance of monomeric antenna subunits in the quenching mechanism (Cazzaniga et al. 2020) but indicate CP26 as the monomeric antenna protein with a prevalent role in NPQ. These results are consistent with previous evidence that points out to CP26 as a docking site for LHCSR3 on PSII supercomplexes (Kim et al. 2017; Semchonok et al. 2017). Being in an external position, CP26 could represent a more accessible point for a direct interaction with LHCSR3, while CP29 is clamped between the core and the S- and M-LHCII (Drop et al. 2014; Cao et al. 2020). The dramatic difference in NPQ between *k6#* and *k9* could be influenced also by the change of expression levels of the remaining monomeric antenna in the single mutants. While in Wt and *k6#* the relative amount of CP29 is similar, *k9* shows an overaccumulation of CP26 protein, with an increase of ∼50% compared to Wt. This compensatory mechanism has never been observed in *Arabidopsis* (*Arabidopsis thaliana*), where the CP29-binding site cannot be occupied by other subunits (de Bianchi et al. 2011). In *A. thaliana*, where the absence of CP26 had no effect on the quenching mechanism, the simultaneous deletion of all monomeric subunits reduced the light-harvesting capacity but had a minor role in NPQ (de Bianchi et al. 2008; Dall'Osto et al. 2020). The interaction between LHCSR and the core complex involves also other PSII subunits. Previous studies have shown that PSBR is necessary for the efficient binding of LHCSR3 to the core complex, and PSBR interacts with PSBP, which is reduced in the *k6#* mutant. Although we were unable to quantify PSBR subunits in our samples, the reduction of PSBP hints at the possibility of a decrease in this subunit as well. Further investigation of the interaction between CP26 and other PSII core subunits will be necessary to gain a more comprehensive understanding of the molecular mechanisms involved and evaluate this hypothesis. However, in the *k9* mutant, where the NPQ was only slightly reduced compared to the Wt case, the PSBP ratio was similar to that in *k6#*, indicating that the reduction in PSBS is not the primary cause of the NPQ phenotype in *k6#* mutants.

The data from this study further confirm the differences between the LHCSR-dependent NPQ observed in *C. reinhardtii* and the PSBS-dependent NPQ in vascular plants. In both cases, LHCSR proteins and PSBS need to interact with LHC proteins to trigger NPQ (Niyogi and Truong 2013; Sacharz et al. 2017): a possible different affinity of LHCSR and PSBS for the specific LHC antenna could explain the different phenotype observed in the LHC mutant in *C. reinhardtii* compared to *A. thaliana*.

In conclusion, these results point out a distinct role of the 2 monomeric antenna subunits in *C. reinhardtii*. While CP29 is fundamental for efficient light harvesting and PSII activity, CP26 plays a major role in NPQ induction. It is important to note that a small NPQ induction at very high light could still be observed in the absence of both CP26 and CP29: this residual NPQ was probably due to the interaction of LHCSR1 or LHCSR3 with LHCII subunits, as previously reported (Kim et al. 2017; Semchonok et al. 2017). These data could be useful to further understand the different NPQ molecular mechanisms in microalgae compared to vascular plants and to identify targets to tune this mechanism to increase productivity under different light regimes.

Materials and methods

Culture conditions

C. reinhardtii CC503 (Wt) and mutant strains were grown at 24 °C in a high-salt (HS) medium (Kropat et al. 2011) on a rotary shaker in Erlenmeyer flasks under continuous illumination with white LED. Cell densities were measured using the Countess II FL Automated Cell Counter (Thermo Fisher Scientific). Single mutants on CP29 (*k9*) and double mutants on CP26 and CP29 (*k69*) were obtained (Cazzaniga et al. 2020).

Generation of *C. reinhardtii* mutants by CRISPR/Cas9 genome editing

To generate knockout CP26 mutants, the CRISPR/Cas9 RNP complex-mediated genome editing method was performed according to Kim et al. (2020a, b) and Joo et al. (2022) (see Supplemental Methods S1). To verify the integration and copy number of the *aphVII* gene in the genome, the genomic DNA was digested by *Kpn*I or *Nco*I, and Southern blot analysis was performed using the *aphVII* gene probe for the detection of DNA integration. Bands were visualized using the Gene Images AlkPhos Direct Labeling and Detection System (Amersham, Little Chalfont, Bucks, UK).

Mutant complementation

The vector used for CP26 knockout mutant complementation was obtained by fusion PCR, merging the 1,000-bp upstream 5′-UTR of the CP29 gene (Cre17.g720250) with the whole CP26 gene (Cre16.g673650) deprived of the promoter region and extended of the 300-bp downstream 3′-UTR. In

the case of CP29 complementation in the *k69* background, the genomic sequence of the CP29 gene from the 1,000-bp upstream of 5′-UTR to the 300-bp downstream of 3′-UTR was used. These sequences were cloned into the pOpt2 vector system and used for transformation. Nuclear transformation was carried out by glass beads as previously described (Perozeni et al. 2020) using 10 μg of linearized plasmids followed by a selection of transformants on TAP agar plates (Kropat et al. 2011) supplied by paromomycin (10 mg/L) for 6 to 7 d. All the primer sequences used are reported in Supplemental Methods S1.

Membrane preparation, gel electrophoresis, and immunoblotting

Thylakoid membranes were isolated as previously described (Bonente et al. 2008). SDS-PAGE analysis was performed using the Tris-Tricine buffer system (Schägger and von Jagow 1987) followed by Coomassie blue staining. For immunotitration, thylakoid samples were loaded for each sample and electroblotted on nitrocellulose membranes; then, proteins were quantified with an alkaline phosphatase–conjugated antibody system. αCP26 (AS09 407), αCP29 (AS04 045), αLHCII (AS01 003) αCP43 (AS11 1787), αPSAA (AS06 172), αLHCSR1 (AS14 2819), αLHCSR3 (AS14 2766), and αPSBP (AS06 167) antibodies were purchased from Agrisera (Sweden). Nondenaturing Deriphat-PAGE was performed following the method developed in Peter et al. (1991). Thylakoids concentrated at 1 mg/mL Chls were solubilized with a final 0.8% (w/v) α-DM, and 30 μg of Chls were loaded in each lane.

Pigment and spectroscopy analysis

Pigments were extracted from intact cells using 80% (v/v) acetone buffered with Na_2CO_3 and analyzed by reverse-phase HPLC (Lagarde et al. 2000) as described in Perozeni et al. (2020). The 77-K fluorescence emission spectra on frozen cells were registered using a BeamBio custom device equipped with a USB2000 Ocean Optics spectrometer (Ocean Optics).

Time-resolved fluorescence on whole cells

Time-resolved fluorescence measurements were carried out using a Ti:sapphire laser (Chameleon Ultra II, Coherent, repetition rate of 80 MHz and 140-fs pulse width). A β-barium borate (BBO) crystal was used to frequency-double the 950-nm laser output in order to generate the 475-nm excitation wavelength. The fluorescence signal from the cells was focused on the entrance slit of a spectrograph (Acton SP2300i, Princeton Instruments). A streak camera (C5680, Hamamatsu), equipped with the Synchroscan sweep module, provides spectral–temporal matrices with spectral and temporal resolutions of ∼1 nm and ∼20 ps, respectively, for the temporal window of 2 ns. A CCD (Hamamatsu ORCA-R2 C10600) recorded the streak image. The measurements were carried out in cuvettes with an optical path length of 10 mm, and the sample was under constant circulation from a reservoir of 30-mL sample volume through a tube and peristaltic pump to avoid any photodamage of the samples.

Measurements of photosynthetic activity

Photosynthetic parameters ΦPSII, qL, ETR, and NPQ were obtained by measuring with a DUAL-PAM-100 fluorometer (Heinz Walz) the Chl fluorescence of intact cells at room temperature in a 1 × 1-cm cuvette mixed by magnetic stirring. ΦPSII, qL, and ETR were measured and calculated according to Baker (2008) and Van Kooten and Snel (1990) upon 20 min of illumination. NPQ measurements were performed on dark-adapted intact cells as described in Cazzaniga et al. (2020) with the following modifications: cells were adapted to high light only for 2 d before NPQ measurements, and far-red light exposure was performed for 2 min before turning on the actinic light. The PSII functional antenna size was measured from fast Chl induction kinetics induced with a red light of 11 μmol photons m^{-2} s^{-1} on dark-adapted cells (∼2 · 10^6 cells/mL) incubated with 50-μM DCMU. The reciprocal of time corresponding to two-thirds of the fluorescence rise (τ2/3) was taken as a measure of the PSII functional antenna size (Malkin et al. 1981). The oxygen evolution activity of the cultures was measured at 25 °C with a Clark-type O_2 electrode (Hansatech), as described previously (Cazzaniga et al. 2020). NPQ acid induction in the dark was induced as previously described (Tian et al. 2019). See Supplemental Methods S1 for additional details.

Statistical analyses

The statistical significance of differences between Wt and mutants was determined by Student's t test ($P < 0.05$). Error bars are standard deviations. Sample sizes are reported for the different experiments in figure legends.

Accession numbers

Sequence data from this article can be found in the GenBank/EMBL data libraries under accession numbers reported in Supplemental Table S5.

Author contributions

M.B. designed the research. E.J. coordinated the research activity for the generation of mutant strains and contributed to the experiment design. C.D. coordinated the research activity for time-resolved fluorescence analysis of whole cells. S.C., M.K., S.S., F.P., and M.P. performed the experiments. All the authors analyzed the data. S.C., E.J., and M.B. wrote the paper. All the authors discussed the results, contributed to the data interpretation, commented on the manuscript, and approved its final version. The author responsible for the distribution of materials integral to the findings presented in this article in accordance with the policy described in the Instructions for Authors (https://academic.oup.com/plphys/pages/General-Instructions) is M.B.

Supplemental data

The following materials are available in the online version of this article.

Supplemental Methods S1. CRISPR/Cas9 genome editing, acid-induced quenching, and primer sequences.

Supplemental Figure S1. Protein sequence alignment of CP26 and CP29 from *C. reinhardtii* and CP29 from spinach.

Supplemental Figure S2. Expression of CP29 in the CP26/CP29 double mutant background.

Supplemental Figure S3. Expression of CP29 in the CP29 single mutant background.

Supplemental Figure S4. Screening and verification of CP26 knockout mutants.

Supplemental Figure S5. CP26 immunotitration in the *k9* mutant.

Supplemental Figure S6. PSBP quantification.

Supplemental Figure S7. F_0 and F_m fluorescence normalized to Chl content.

Supplemental Figure S8. Photosynthetic parameters in *k9* and *k69*.

Supplemental Figure S9. Growth curves for *k9* and *k69*.

Supplemental Figure S10. Immunotitration of LHCSR proteins per PSII.

Supplemental Figure S11. NPQ at different actinic light intensities.

Supplemental Figure S12. NPQ in *k9* and *k69* mutants.

Supplemental Figure S13. Acid-induced quenching in 4a+ and *npq4 lhcsr1*.

Supplemental Figure S14. Acid-induced quenching in *k9* and *k69*.

Supplemental Figure S15. *k6#* mutant complementation.

Supplemental Figure S16. *k6#* line complemented with CP26.

Supplemental Figure S17. Photosynthetic electron flow with complemented lines.

Supplemental Figure S18. Growth curves under autotrophic conditions with complemented lines.

Supplemental Table S1. Sanger sequencing of the CP26 knockout mutants.

Supplemental Table S2. Fluorescence lifetimes of whole *C. reinhardtii* cells.

Supplemental Table S3. Light curve parameters and respiration rates.

Supplemental Table S4. Pigment analysis and F_v/F_m of the complemented lines.

Supplemental Table S5. Accession numbers of genes mentioned in this work.

Funding

The research was supported by the ERC (European Research Council) Starting Grant SOLENALGAE (679814) to M.B. and by the Basic Science Research Program (NRF2020R1A2C2011998) of the National Research Foundation (NRF) of Korea to E.J.

Conflict of interest statement. The authors declare that the research was conducted in the absence of any commercial or financial relationships that could be construed as potential conflicts of interest.

Data availability

The data that support the findings of this study are available from the corresponding author upon reasonable request. The strains herein investigated are made available by the corresponding author upon request.

References

Albanese P, Melero R, Engel BD, Grinzato A, Berto P, Manfredi M, Chiodoni A, Vargas J, Sorzano CÓS, Marengo E, et al. Pea PSII-LHCII supercomplexes form pairs by making connections across the stromal gap. Sci Rep. 2017:**7**(1):10067. https://doi.org/10.1038/s41598-017-10700-8

Allorent G, Tokutsu R, Roach T, Peers G, Cardol P, Girard-Bascou J, Seigneurin-Berny D, Petroutsos D, Kuntz M, Breyton C, et al. A dual strategy to cope with high light in *Chlamydomonas reinhardtii*. Plant Cell. 2013:**25**(2):545–557. https://doi.org/10.1105/tpc.112.108274

Aro E-M, Virgin I, Andersson B. Photoinhibition of photosystem II—inactivation, protein damage and turnover. Biochim Biophys Acta. 1993:**1143**(2):113–134. https://doi.org/10.1016/0005-2728(93)90134-2

Baek K, Kim DH, Jeong J, Sim SJ, Melis A, Kim JS, Jin E, Bae S. DNA-free two-gene knockout in *Chlamydomonas reinhardtii* via CRISPR-Cas9 ribonucleoproteins. Sci Rep. 2016:**6**:30620. https://doi.org/10.1038/srep30620

Baker NR. Chlorophyll fluorescence: a probe of photosynthesis in vivo. Annu Rev Plant Biol. 2008:**59**(1):89–113. https://doi.org/10.1146/annurev.arplant.59.032607.092759

Ballottari M, Truong TB, De Re E, Erickson E, Stella GR, Fleming GR, Bassi R, Niyogi KK. Identification of pH-sensing sites in the light harvesting complex stress-related 3 protein essential for triggering non-photochemical quenching in *Chlamydomonas reinhardtii*. J Biol Chem. 2016:**291**(14):7334–7346. https://doi.org/10.1074/jbc.M115.704601

Bernaerts T, Gheysen L, Foubert I, Hendrickx M, Van Loey A. The potential of microalgae and their biopolymers as structuring ingredients in food: a review. Biotechnol Adv . 2019:**37**(8):107419. https://doi.org/10.1016/j.biotechadv.2019.107419

Bonente G, Howes BD, Caffarri S, Smulevich G, Bassi R. Interactions between the photosystem II subunit PsbS and xanthophylls studied in vivo and in vitro. J Biol Chem. 2008:**283**(13):8434–8445. https://doi.org/10.1074/jbc.M708291200

Butler WL. Primary photochemistry of photosystem II in photosynthesis. Acc Chem Res. 1973:**6**(6):177–184. https://doi.org/10.1021/ar50066a001

Caffarri S, Passarini F, Bassi R, Croce R. A specific binding site for neoxanthin in the monomeric antenna proteins CP26 and CP29 of photosystem II. FEBS Lett. 2007:**581**(24):4704–4710. https://doi.org/10.1016/j.febslet.2007.08.066

Camacho F, Macedo A, Malcata F. Potential industrial applications and commercialization of microalgae in the functional food and feed industries: a short review. Mar Drugs. 2019:**17**(6):312. https://doi.org/10.3390/md17060312

Cao P, Pan X, Su X, Liu Z, Li M. Assembly of eukaryotic photosystem II with diverse light-harvesting antennas. Curr Opin Struct Biol. 2020:**63**:49–57. https://doi.org/10.1016/j.sbi.2020.03.007

Cazzaniga S, Kim M, Bellamoli F, Jeong J, Lee S, Perozeni F, Pompa A, Jin E, Ballottari M. Photosystem II antenna complexes CP26 and

CP29 are essential for nonphotochemical quenching in *Chlamydomonas reinhardtii*. Plant Cell Environ. 2020:**43**(2):496–509. https://doi.org/10.1111/pce.13680

Croce R, Van Amerongen H. Light-harvesting and structural organization of photosystem II: from individual complexes to thylakoid membrane. J Photochem Photobiol B. 2011:**104**(1–2):142–153. https://doi.org/10.1016/j.jphotobiol.2011.02.015

Dall'Osto L, Cazzaniga S, Zappone D, Bassi R. Monomeric light harvesting complexes enhance excitation energy transfer from LHCII to PSII and control their lateral spacing in thylakoids. Biochim Biophys Acta Bioenerg. 2020:**1861**(4):148035. https://doi.org/10.1016/j.bbabio.2019.06.007

de Bianchi S, Betterle N, Kouril R, Cazzaniga S, Boekema E, Bassi R, Dall'Osto L. *Arabidopsis* mutants deleted in the light-harvesting protein Lhcb4 have a disrupted photosystem II macrostructure and are defective in photoprotection. Plant Cell. 2011:**23**(7):2659–2679. https://doi.org/10.1105/tpc.111.087320

de Bianchi S, Dall'Osto L, Tognon G, Morosinotto T, Bassi R. Minor antenna proteins CP24 and CP26 affect the interactions between photosystem II subunits and the electron transport rate in grana membranes of *Arabidopsis*. Plant Cell. 2008:**20**(4):1012–1028. https://doi.org/10.1105/tpc.107.055749

Dinc E, Tian L, Roy LM, Roth R, Goodenough U, Croce R. LHCSR1 induces a fast and reversible pH-dependent fluorescence quenching in LHCII in *Chlamydomonas reinhardtii* cells. Proc Natl Acad Sci U S A. 2016:**113**(27):7673–7678. https://doi.org/10.1073/pnas.1605380113

Drop B, Webber-Birungi M, Yadav SK, Filipowicz-Szymanska A, Fusetti F, Boekema EJ, Croce R. Light-harvesting complex II (LHCII) and its supramolecular organization in *Chlamydomonas reinhardtii*. Biochim Biophys Acta. 2014:**1837**(1):63–72. https://doi.org/10.1016/j.bbabio.2013.07.012

Elrad D, Niyogi KK, Grossman AR. A major light-harvesting polypeptide of photosystem II functions in thermal dissipation. Plant Cell. 2002:**14**(8):1801–1816. https://doi.org/10.1105/tpc.002154

Erickson E, Wakao S, Niyogi KK. Light stress and photoprotection in *Chlamydomonas reinhardtii*. Plant J. 2015:**82**(3):449–465. https://doi.org/10.1111/tpj.12825

Garnier J, Maroc J, Guyon D. Low-temperature fluorescence emission spectra and chlorophyll-protein complexes in mutants of *Chlamydomonas reinhardtii*: evidence for a new chlorophyll-a-protein complex related to photosystem I. Biochim Biophys Acta. 1986:**851**(3):395–406. https://doi.org/10.1016/0005-2728(86)90076-9

Genty B, Briantais J-M, Baker NR. The relationship between the quantum yield of photosynthetic electron transport and quenching of chlorophyll fluorescence. Biochim Biophys Acta. 1989:**990**(1):87–92. https://doi.org/10.1016/S0304-4165(89)80016-9

Girolomoni L, Ferrante P, Berteotti S, Giuliano G, Bassi R, Ballottari M. The function of LHCBM4/6/8 antenna proteins in *Chlamydomonas reinhardtii*. J Exp Bot. 2017:**68**(3):627–641. https://doi.org/10.1093/jxb/erw462

Głowacka K, Kromdijk J, Kucera K, Xie J, Cavanagh AP, Leonelli L, Leakey ADB, Ort DR, Niyogi KK, Long SP. Photosystem II subunit S overexpression increases the efficiency of water use in a field-grown crop. Nat Commun. 2018:**9**(1):868. https://doi.org/10.1038/s41467-018-03231-x

Graham PJ, Nguyen B, Burdyny T, Sinton D. A penalty on photosynthetic growth in fluctuating light. Sci Rep. 2017:**7**(1):12513. https://doi.org/10.1038/s41598-017-12923-1

Hill R, Scarisbrick R. Production of oxygen by illuminated chloroplasts. Nature. 1940:**146**(3689):61. https://doi.org/10.1038/146061a0

Horton P. Nonphotochemical quenching of chlorophyll fluorescence. In: **Jennings RC**, editors. Light as an energy source and information carrier in plant physiology. New York: Plenum Press; 1996. p. 99–111.

Ido K, Nield J, Fukao Y, Nishimura T, Sato F, Ifuku K. Cross-linking evidence for multiple interactions of the PsbP and PsbQ proteins in a higher plant photosystem II supercomplex. J Biol Chem. 2014:**289**(29):20150–20157. https://doi.org/10.1074/jbc.M114.574822

Joo S, Kariyawasam T, Kim M, Jin E, Goodenough U, Lee JH. Sex-linked deubiquitinase establishes uniparental transmission of chloroplast DNA. Nat Commun. 2022:**13**(1):1133. https://doi.org/10.1038/s41467-022-28807-6

Kim E, Akimoto S, Tokutsu R, Yokono M, Minagawa J. Fluorescence lifetime analyses reveal how the high light-responsive protein LHCSR3 transforms PSII light-harvesting complexes into an energy-dissipative state. J Biol Chem. 2017:**292**(46):18951–18960. https://doi.org/10.1074/jbc.M117.805192

Kim J, Lee S, Baek K, Jin E. Site-specific gene knock-out and on-site heterologous gene overexpression in *Chlamydomonas reinhardtii* via a CRISPR-Cas9-mediated knock-in method. Front Plant Sci. 2020b:**11**:306. https://doi.org/10.3389/fpls.2020.00306

Kim E, Watanabe A, Duffy CDP, Ruban AV, Minagawa J. Multimeric and monomeric photosystem II supercomplexes represent structural adaptations to low- and high-light conditions. J Biol Chem. 2020a:**295**(43):14537–14545. https://doi.org/10.1074/jbc.RA120.014198

Koyande A, Chew K, Rambabu K, Tao Y, Chu D, Show P. Microalgae: a potential alternative to health supplementation for humans. Food Sci Hum Wellness. 2019:**8**(1):16–24. https://doi.org/10.1016/j.fshw.2019.03.001

Kromdijk J, Glowacka K, Leonelli L, Gabilly ST, Iwai M, Niyogi KK, Long SP. Improving photosynthesis and crop productivity by accelerating recovery from photoprotection. Science. 2016:**354**(6314):857–861. https://doi.org/10.1126/science.aai8878

Kropat J, Hong-Hermesdorf A, Casero D, Ent P, Castruita M, Pellegrini M, Merchant S, Malasarn D. A revised mineral nutrient supplement increases biomass and growth rate in *Chlamydomonas reinhardtii*. Plant J. 2011:**66**(5):770–780. https://doi.org/10.1111/j.1365-313X.2011.04537.x

Lagarde D, Beuf L, Vermaas W. Increased production of zeaxanthin and other pigments by application of genetic engineering techniques to *Synechocystis sp.* strain PCC 6803. Appl Environ Microbiol. 2000:**66**(1):64–72. https://doi.org/10.1128/AEM.66.1.64-72.2000

Liguori N, Roy LM, Opacic M, Durand G, Croce R. Regulation of light harvesting in the green alga *Chlamydomonas reinhardtii*: the C-terminus of LHCSR is the knob of a dimmer switch. J Am Chem Soc. 2013:**135**(49):18339–18342. https://doi.org/10.1021/ja4107463

Liu Z, Yan H, Wang K, Kuang T, Zhang J, Gui L, An X, Chang W. Crystal structure of spinach major light-harvesting complex at 2.72 A resolution. Nature. 2004:**428**(6980):287–292. https://doi.org/10.1038/nature02373

Long SP, Humphries S, Falkowski PG. Photoinhibition of photosynthesis in nature. Ann Rev Plant Physiol Plant Mol Biol. 1994:**45**(1):633–662. https://doi.org/10.1146/annurev.pp.45.060194.003221

Malkin S, Armond PA, Mooney HA, Fork DC. Photosystem II photosynthetic unit sizes from fluorescence induction in leaves: correlation to photosynthetic capacity. Plant Physiol. 1981:**67**(3):570–579. https://doi.org/10.1104/pp.67.3.570

Medipally SR, Yusoff FM, Banerjee S, Shariff M. Microalgae as sustainable renewable energy feedstock for biofuel production. Biomed Res Int. 2015:**2015**:519513. https://doi.org/10.1155/2015/519513

Minagawa J, Takahashi Y. Structure, function and assembly of photosystem II and its light-harvesting proteins. Photosynth Res. 2004:**82**(3):241–263. https://doi.org/10.1007/s11120-004-2079-2

Natali A, Croce R. Characterization of the major light-harvesting complexes (LHCBM) of the green alga *Chlamydomonas reinhardtii*. PLoS One. 2015:**10**(2):e0119211. https://doi.org/10.1371/journal.pone.0119211

Neidhardt J, Benemann JR, Zhang LP, Melis A. Photosystem-II repair and chloroplast recovery from irradiance stress: relationship between chronic photoinhibition, light-harvesting chlorophyll antenna size and photosynthetic productivity in *Dunaliella salina* (green algae).

Photosynthesis Res. 1998:**56**(2):175–184. https://doi.org/10.1023/A:1006024827225

Niyogi KK, Truong TB. Evolution of flexible non-photochemical quenching mechanisms that regulate light harvesting in oxygenic photosynthesis. Curr Opin Plant Biol. 2013:**16**(3):307–314. https://doi.org/10.1016/j.pbi.2013.03.011

Pan X, Li M, Wan T, Wang L, Jia C, Hou Z, Zhao X, Zhang J, Chang W. Structural insights into energy regulation of light-harvesting complex CP29 from spinach. Nat Struct Mol Biol. 2011:**18**(3):309–315. https://doi.org/10.1038/nsmb.2008

Peers G, Truong TB, Ostendorf E, Busch A, Elrad D, Grossman AR, Hippler M, Niyogi KK. An ancient light-harvesting protein is critical for the regulation of algal photosynthesis. Nature. 2009:**462**(7272):518–521. https://doi.org/10.1038/nature08587

Perozeni F, Cazzaniga S, Baier T. Turning a green alga red: engineering astaxanthin biosynthesis by intragenic pseudogene revival in *Chlamydomonas reinhardtii*. Plant Biotechnol J. 2020:**18**(10):2053–2067. https://doi.org/10.1111/pbi.13364

Peter GF, Takeuchi T, Thornber JP. Solubilization and two-dimensional electrophoretic procedures for studying the organization and composition of photosynthetic membrane polypeptides. Methods: Companion Methods Enzymol. 1991:**3**(2):115–124. https://doi.org/10.1016/S1046-2023(05)80203-8

Rani A, Saini KC, Bast F, Mehariya S, Bhatia SK, Lavecchia R, Zuorro A. Microorganisms: a potential source of bioactive molecules for antioxidant applications. Molecules. 2021:**26**(4):1142. https://doi.org/10.3390/molecules26041142

Sacharz J, Giovagnetti V, Ungerer P, Mastroianni G, Ruban AV. The xanthophyll cycle affects reversible interactions between PsbS and light-harvesting complex II to control non-photochemical quenching. Nat Plants. 2017:**3**:16225. https://doi.org/10.1038/nplants.2016.225

Schägger H, von Jagow G. Tricine-sodium dodecyl sulfate-polyacrylamide gel electrophoresis for the separation of proteins in the range from 1 to 100 kDa. Anal Biochem. 1987:**166**(2):368–379. https://doi.org/10.1016/0003-2697(87)90587-2

Semchonok DA, Sathish Yadav KN, Xu P, Drop B, Croce R, Boekema EJ. Interaction between the photoprotective protein LHCSR3 and C2S2 photosystem II supercomplex in *Chlamydomonas reinhardtii*. Biochim Biophys Acta. 2017:**1858**(5):379–385. https://doi.org/10.1016/j.bbabio.2017.02.015

Shen L, Huang Z, Chang S, Wang W, Wang J, Kuang T, Han G, Shen J-R, Zhang X. Structure of a C2S2M2N2-type PSII–LHCII supercomplex from the green alga *Chlamydomonas reinhardtii*. Proc Natl Acad of Sci U S A. 2019:**116**(42):21246–21255. https://doi.org/10.1073/pnas.1912462116

Suga M, Akita F, Hirata K, Ueno G, Murakami H, Nakajima Y, Shimizu T, Yamashita K, Yamamoto M, Ago H, et al. Native structure of photosystem II at 1.95 A resolution viewed by femtosecond X-ray pulses. Nature. 2015:**517**(7532):99–103. https://doi.org/10.1038/nature13991

Tian L, Nawrocki Wojciech J, Liu X, Polukhina I, van Stokkum Ivo HM, Croce R. pH dependence, kinetics and light-harvesting regulation of nonphotochemical quenching in *Chlamydomonas*. Proc Natl Acad Sci U S A. 2019:**116**(17):8320–8325. https://doi.org/10.1073/pnas.1817796116

Tokutsu R, Kato N, Bui KH, Ishikawa T, Minagawa J. Revisiting the supramolecular organization of photosystem II in *Chlamydomonas reinhardtii*. J Biol Chem. 2012:**287**(37):31574–31581. https://doi.org/10.1074/jbc.M111.331991

Tokutsu R, Minagawa J. Energy-dissipative supercomplex of photosystem II associated with LHCSR3 in *Chlamydomonas reinhardtii*. Proc Natl Acad Sci U S A. 2013:**110**(24):10016–10021. https://doi.org/10.1073/pnas.1222606110

Troiano JM, Perozeni F, Moya R, Zuliani L, Baek K, Jin E, Cazzaniga S, Ballottari M, Schlau-Cohen GS. Identification of distinct pH- and zeaxanthin-dependent quenching in LHCSR3 from *Chlamydomonas reinhardtii*. Elife. 2021:**10**:e60383. https://doi.org/10.7554/eLife.60383

Van Kooten O, Snel JFH. The use of chlorophyll fluorescence nomenclature in plant stress physiology. Photosynt Res. 1990:**25**(3):147–150. https://doi.org/10.1007/BF00033156

Vass I, Styring S, Hundal T, Koivuniemi A, Aro E-M, Andersson B. Reversible and irreversible intermediates during photoinhibition of photosystem II: stable reduced QA species promote chlorophyll triplet formation. Proc Natl Acad Sci U S A. 1992:**89**(4):1408–1412. https://doi.org/10.1073/pnas.89.4.1408